Numerical calculations of multiphoton molecular absorption

Brian Kaufman,[1] Philipp Marquetand,[2,3,4] Thomas Weinacht,[1] and Tamás Rozgonyi[5]
[1]*Department of Physics and Astronomy, Stony Brook University, Stony Brook, New York 11794-3800, USA*
[2]*Faculty of Chemistry, Institute of Theoretical Chemistry, University of Vienna, Währinger Strasse 17, 1090 Wien, Austria*
[3]*Vienna Research Platform on Accelerating Photoreaction Discovery, University of Vienna, Währinger Strasse 17, 1090 Wien, Austria*
[4]*Faculty of Chemistry, Data Science at Uni Vienna, University of Vienna, Währinger Strasse 29, 1090 Wien, Austria*
[5]*Wigner Research Centre for Physics, P.O. Box 49, H-1525 Budapest, Hungary*

(Received 4 April 2022; accepted 29 June 2022; published 19 July 2022)

Motivated by the possibility of multiphoton-driven pump-probe experiments, such as time-resolved photoelectron spectroscopy, we carry out essential states's calculations of strong-field molecular excitation by solving the time-dependent Schrödinger equation for a molecule in a high-intensity laser field. Usually such calculations rely on adiabatic elimination, but here we make direct use of a large number of energies and transition dipole moments obtained from electronic structure calculations. In this way, we capture a range of multiphoton absorption orders, from 2 to 5, and include dynamic Stark shifts naturally. We consider a range of laser frequencies and intensities to characterize several multiphoton resonances and dynamic Stark shifts. The calculations also include averaging over molecular orientation and geometry, but are carried out for frozen nuclei, which is relevant in the limit of very short laser pulses (<10 fs). Here we focus on the molecule thiophene; however, these calculations can easily be implemented for other molecules with appropriate electronic structure input.

DOI: 10.1103/PhysRevA.106.013111

I. INTRODUCTION

While linear ("single photon") absorption spectroscopy, described in terms of first-order perturbation theory, has proven to be enormously successful in characterizing and identifying different molecules [1], multiphoton absorption offers a number of unique possibilities that yield information not available via single-photon absorption measurements [2–4]. These include a wide range of experiments from pump-probe measurements that make use of two linear absorption processes (overall second order in the applied electric field strength) to follow dynamics on an excited state of the molecule [5,6], to resonance-enhanced multiphoton photoionization (REMPI), which provides information on highly excited states [7], all the way to two photon microscopy experiments that allow for more localized probing of samples than linear absorption would provide [8]. While approaches such as adiabatic elimination allow for a clear analytical framework for describing multiphoton absorption or decay in terms of a few essential states [9–14], it is a nontrivial task to carry out calculations of the coupling strengths and Stark shifts because the calculations above second order involve nested sums over a large number of states. Furthermore, adiabatic elimination breaks down for very short pulses where the bandwidth of the laser includes frequencies that drive resonant coupling between many states [15]. Finally, a conceptual difference between using adiabatic elimination and solving the time-dependent Schrödinger equation (TDSE) for the full system is that in our present case we consider all the photon orders at the same time and do not just provide a formula for, e.g., the third or fourth and so on order absorption. In the case of adiabatic elimination one should know *a priori* which states one can ignore, and for this one should know which order of absorption one "has to" compute, i.e., which one will be the relevant one for a given measurement.

A simpler approach than adiabatic elimination is commonly used to calculate linear absorption spectra and is implemented in many quantum chemistry packages [16–19] in the form of oscillator strengths. Here, a first approximation to the linear absorption spectrum is computed as a stick spectrum which consists of an excited state's energies and corresponding oscillator strengths at the ground-state equilibrium geometry. Such a stick spectrum then needs to be convoluted, e.g., with Gaussians of a manually adapted width to match the experimental line broadening. Using more than one geometry in such a calculation is termed the nuclear ensemble approach and can substantially improve the prediction quality of linear absorption spectra [20–22]. In these approaches, the nuclei are kept fixed and a delta-pulse excitation is assumed. Multiphoton excitation is not described in these approaches.

Here, we go beyond the calculation of oscillator strengths and instead solve the TDSE with a short, explicit laser interaction included to describe multiphoton absorption. In a precursor step, we make use of electronic structure calculations to determine the energies and dipole couplings of the first $\sim$30 states of a molecule (the "essential states" necessary to capture the strong field-driven population dynamics). This information enters the TDSE calculations. Here, we choose to keep the nuclei frozen to keep the computations tractable, but still go beyond the linear absorption regime. This treatment of the light-matter coupling is well suited for very short pulse

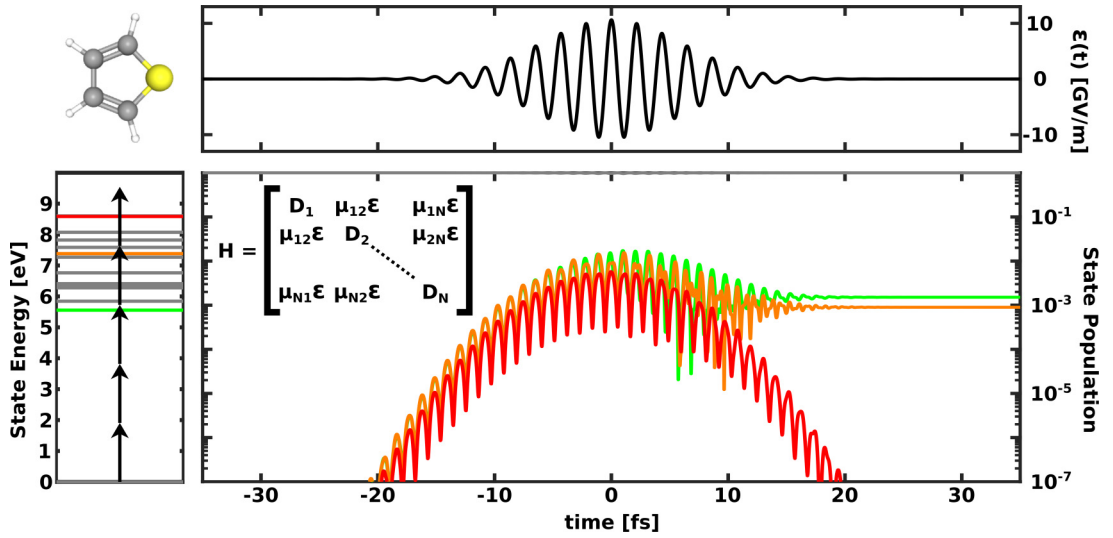

FIG. 1. Solving the TDSE for thiophene (molecular cartoon in top left) including light-matter coupling. The electronic states presented in the bottom left panel are calculated *ab initio* from the electronic structure at the Franck-Condon geometry. Multiphoton arrows are shown in black to indicate the multiphoton transitions occurring: three-photon excitation to state 1 (green), four-photon to state 8 (orange), and five-photon to state 13 (red). A 10-fs laser pulse with an intensity of 15 TW/cm^2 at a central wavelength of 650 nm is shown in the top right panel. The bottom panel shows the state populations on a log scale as a function of time. The states with significant population transfer are shown. We show the full Hamiltonian H, where $D_N = E_N + \mu_{NN}\epsilon$.

durations (<10 fs), during which nuclear motion is minimal, and for which there are laser couplings between many pairs of states such that the number of essential states is significant (i.e., $\gg$3).

We consider rotational averaging to provide results that are relevant to experiments that do not work with a well-aligned molecular sample. We also consider a Wigner distribution of molecular geometries about the equilibrium geometry of the electronic ground state of the neutral molecule [for simplicity referred to here as the Franck-Condon (FC) geometry] to account for the spread of the initial N-dimensional vibrational wave function. Furthermore, by sampling different geometries within the Wigner distribution, we capture some coupling between different electronic states (e.g., intensity borrowing).

While essential states calculations were carried out before, in this work we aim to set the stage for time-resolved experiments that can probe nonadiabatic excited state dynamics. The idea is that a single broadband (∼5 fs) laser pulse can be shaped to generate a pump-probe pulse pair, with the "pump" pulse launching an excited state wave packet and the "probe" pulse ionizing the molecule in a multiphoton-pump multiphoton-probe time-resolved photoelectron spectroscopy (TRPES) experiment [23,24]. Two major advantages of this multiphoton-pump approach are that one can potentially study optically dark states that are not accessible with single-photon absorption and one can use the high time resolution available from near-IR and optical pulses to probe nonadiabatic dynamics in multiple excited states in parallel [23,25].

Our calculations are carried out for thiophene [26], which is an aromatic five-membered ring and plays an important role in organic chemistry. Thiophene and its derivatives are building blocks of very promising organic materials for technological applications [27], such as organic solar cells [28,29], light-emitting diodes [30], and field-effect transistors [31]. Consequently, the excited states of thiophene and their photophysics are of considerable interest, see Refs. [32–36].

The computations, performed here for thiophene, utilize the electronic Hamiltonian within the fixed nuclei approximation. The electronic structure calculations account for the multielectron nature of the wave function, and since nuclear dynamics are not considered, this leaves only the energies and couplings between states for the light-matter interaction. Therefore, the computations can easily be extended to almost any other molecule of similar size and structure.

Figure 1 shows a cartoon diagram of thiophene and illustrates the basic ideas behind the calculations, which are described in detail below. In short, we make use of electronic structure calculations to determine the energies (E) of the first 30 electronic states of thiophene (illustrated in the left panel) and the transition dipole moments (μ) between them at the FC geometry (i.e., minimum on the ground electronic state S_0). Along with the applied laser pulse (ϵ), shown in the top right panel, these form the Hamiltonian written in the bottom right panel. We make use of this Hamiltonian to solve the TDSE with nuclear degrees of freedom frozen. Neglecting nuclear dynamics during the pulse can be reasonable if the pulse duration is shorter than the fastest vibrational period [37], although there are some subtleties associated with this for very strong fields where the nuclear coordinate dependence of the coupling between electronic states cannot be ignored [38]. The output of the calculations are the time-dependent populations for each state, shown in the bottom right panel, using a color coding established in the bottom left panel.

II. CALCULATIONS

A. Quantum chemistry

We start with the electronic structure calculations, which were performed with the multistate complete active space perturbation theory second-order (MS-CASPT2) method [39] based on multiconfigurational state-averaged complete active space self-consisted field (SA-CASSCF) reference wave functions. The MS-CASPT2 method was chosen because of its reliability and the possibility of a straightforward systematic improvement of the level of theory. MS-CASPT2 was already successfully used to describe the electronic excited states of thiophene by several groups [35,40,41]. In most of the present computations, the active space included 10 electrons distributed on 11 orbitals and the averaging was performed over 30 electronic states, but in some cases computations were performed with 13 active orbitals or with fewer states to test the role of the active space size and that of the number of states. In each case, state averaging was performed. The shapes of the active orbitals at the FC position are given in the Appendix for the case of 11 orbitals and 30 states.

As an electronic basis, the atomic natural orbital-relativistic correlation consistent (ANO-RCC) basis set [42,43] was used with the following contractions: $5s4p2d1f$ for S, $4s3p2d1f$ for C, and $3s2p1d$ for H atoms. This basis set, together with the above active space, is appropriate to describe the majority of the valence excited states and reproduces the measured linear absorption spectrum very well (see Fig. 12). The description of all the valence and Rydberg states that may contribute to multiphoton processes would requiree either a much larger active space space, resulting in enormous computational cost, or separate computations with different properly designed smaller, active spaces. Although the latter approach was successfully applied for thiophene in Ref. [40] for the totally symmetric FC geometry, this approach could not be followed in the present study in which MS-CASPT2 computations were performed for many asymmetric geometries.

As spin-orbit coupling is small for this system and the pulse durations are short compared to nuclear dynamics, we restricted our investigations to electron dynamics excluding both nonadiabatic effects and intersystem crossings. Accordingly, only singlet states were included in the computations.

We used OPEN-MOLCAS 20.10 [19] and employed the second-order Douglas-Kroll-Hess (DKH) Hamiltonian [44] with the standard (0.25 hartree) ionization potential electron affinity shift and an additional 0.3 hartree imaginary level shift. The transition dipole moment matrix was determined according to the restricted active space state interaction (RASSI) formalism [45].

The FC geometry and normal vibrational modes in the ground electronic state were obtained by density functional theory using the Becke, 3-parameter, Lee-Yang-Parr (B3LYP) functional [46,47] and aug-cc-pVTZ basis set [48]. For this the GAUSSIAN'09 package of programs was used [49]. Wigner sampling of initial geometries were then based on normal mode analysis and 200 different geometries were selected randomly according to the Wigner distribution using the WIGNER.PY routine of the SHARC 2.1 program package [50]. The set of energies and (transition) dipole moments obtained in this way were then employed in the subsequent quantum dynamics simulations.

B. Quantum dynamics

To study the strong-field light-matter interaction, we solve the TDSE

$$i\hbar\frac{\partial\Psi(t,r,R)}{\partial t} = [H_0(r,R) + \vec{\mu}(r,R)\cdot\vec{\epsilon}(t)]\Psi(t,r,R), \quad (1)$$

in MATLAB using the ODE45 differential equation solver, which relies on an explicit Runge-Kutta (4,5) formula. The Hamiltonian, $H = H_0(r,R) + \vec{\mu}(r,R)\cdot\vec{\epsilon}(t)$, shown in Fig. 1, is composed of state energies E via the field-free Hamiltonian H_0, transition dipole moments μ, and electric field ϵ, where we employ the length gauge for the light-matter interaction. Both the state energies and transition dipole moments are calculated from electronic structure calculations. The strength of the electric field $\vec{\epsilon}(t)$ is described by a Gaussian envelope times a cosine wave

$$\vec{\epsilon}(t) = \vec{\epsilon}_0 e^{-4\ln(2)t^2/2\tau^2}\cos(\omega t), \quad (2)$$

where ϵ_0 is the field amplitude, ω is the laser frequency, and τ is the intensity full width at half maximum (FWHM). We use a pulse duration of $\tau = 10$ fs, with an eye towards measurements that can resolve the fastest vibrational dynamics.

The wave function Ψ is a function of the electronic and nuclear coordinates r and R, respectively, and we define it as

$$\Psi(t,r,R) = \sum_i a_i(t)\,|\psi_i(r,R)\rangle\,. \quad (3)$$

For our calculations, we work with fixed nuclear position R_0, and thus $\psi_i(r,R_0)$ is the ith electronic eigenfunction at fixed nuclear position, $R = R_0$, and the absolute square of the complex time-dependent coefficient $a_i(t)$ is the population of this state at time t, the asymptotic values of which are the central quantities of the present investigations. The elements of the transition dipole moment matrix are given by $\vec{\mu}_{ij}(R) = \langle\psi_i(r,R)|\,\vec{\mu}(r,R)\,|\psi_j(r,R)\rangle$.

With the electronic structure calculations in hand and operating in the frozen nuclei regime, our goal is to solve Eq. (1) for the time-dependent coefficients $a_i(t)$:

$$i\hbar\dot{a}_i(t) = \sum_i a_i(t)\,\langle\psi_j(r,R)|\,H\,|\psi_i(r,R)\rangle\,. \quad (4)$$

III. RESULTS AND DISCUSSION

Figure 1 shows the results of a single calculation. Below the cartoon of the molecule in the top left corner is a diagram of the state energies for the first 30 states below the ionization potential $I_p = 8.9$ eV. Five black arrows show multiphoton resonances for a laser pulse with a central wavelength of 650 nm. The top right panel shows the electric field as a function of time for a laser pulse with an intensity of 15 TW/cm^2 and a pulse duration of 10 fs. In the bottom right panel are the state populations as a function of time ($|a(t)|^2$) from solving the TDSE, shown on a log scale for all the states given in the energy diagram. Most states do not come into resonance, so their populations are approximately zero; however, there are

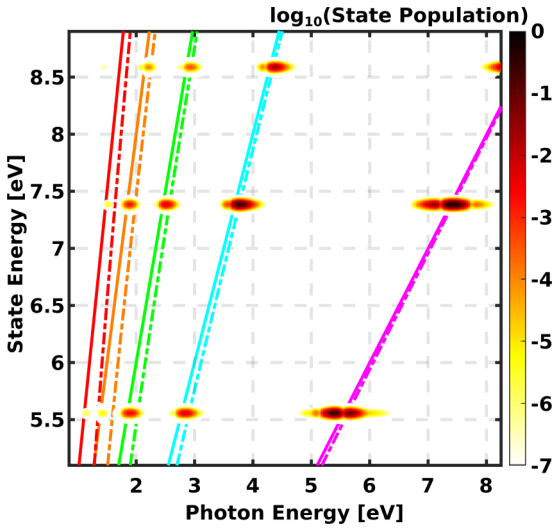

FIG. 2. Multiphoton spectrum: Final-state populations from solving the TDSE for various laser frequencies (photon energies), plotted as a function of state energy and photon energy for a 10-fs pulse with an intensity of 15 TW/cm^2. Multiphoton orders are represented by the diagonal lines: one-photon in magenta; two-photons in cyan; three-photons in green; four-photons in orange; and five-photons in red. Solid lines correspond to $E = nh\nu$ and dashed lines correspond to $E = nh\nu - U_p$. These calculations were carried out for the FC geometry with the laser polarization aligned along the x direction of the molecule (as defined by the central cartoon of Fig. 3).

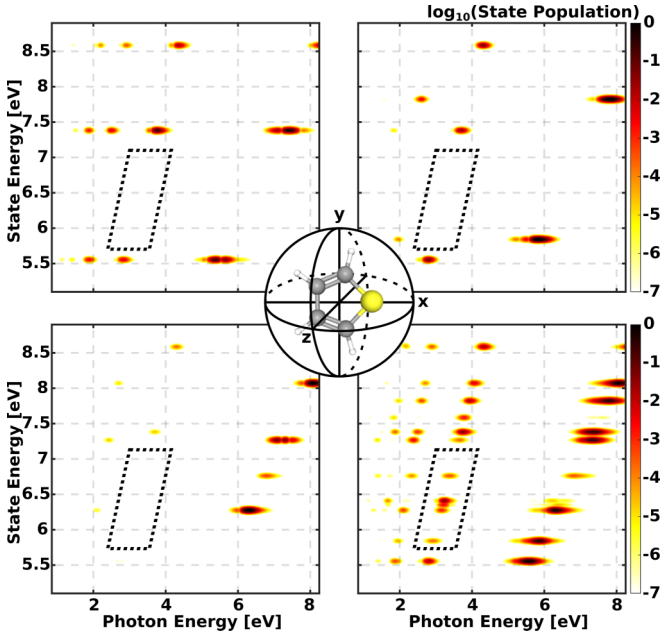

FIG. 3. Multiphoton spectra for different laser-molecule projections in the FC geometry with a 15 TW/cm^2, 10-fs pulse. Top left: x projection; top right: y projection; and bottom left: z projection. Bottom right: Populations averaged for polarizations projected over the full sphere. The dashed box highlights that rotationally averaging is necessary in some cases and goes beyond the sum of the three projections.

three states that populate during the pulse. These are depicted in green, orange, and red. These population curves are color coded to match the states on the left. The green curve corresponds to the state at 5.6 eV, which comes into three-photon resonance, the orange curve corresponds to a state which comes into four-photon resonance around 7.4 eV, and the red curve represents a five-photon off-resonant intermediate state at 8.6 eV, which is why there is no population remaining in the state after the pulse turns off. This specific wavelength in Fig. 1 was chosen to illustrate the nature of the calculations and highlight the fact that there are some multiphoton resonances leaving the population in the state at the end of the pulse, some of-resonant states that are only populated during the pulse, and rapid oscillations that one neglects if one performs adiabatic elimination. Solving the TDSE exactly inherently includes multiphoton couplings between the states.

The calculation shown in Fig. 1 is carried out for a single-photon energy (wavelength). We can extend these results by scanning over a large range of photon energies as represented in Fig. 2. Here we present a "multiphoton spectrum" which shows the final state populations as a function of state and photon energies. Once again we used a 10-fs pulse with an intensity of 15 TW/cm^2. As in Fig. 1, we see population transfer as a result of several multiphoton resonances. Figure 2 serves as a starting point, from which we buildup the physics of this work.

The multiphoton orders are depicted by the diagonal lines: one photon in magenta, two photon in cyan, three photon in green, four photon in orange, and five photon in red. For each photon order, we show two lines: a solid line corresponding to the unshifted energy ($E = nh\nu$) and a dashed line corresponding to the ponderomotive shifted energy ($E = nh\nu - U_p$ where $U_p = \frac{e^2\varepsilon^2}{4m\omega^2}$, with e and m being the charge and mass of the electron). We note that Fig. 2 uses a logarithmic scale to show populations over a large range of values.

A. Rotational averaging

The transition dipole moment μ is a vector quantity, as is the laser field. For a randomly oriented molecular ensemble, one needs to average over different projections of the laser polarization onto the molecular axes, and thus the transition dipole moment for each pair of states is $\vec{\mu_{ij}} \cdot \vec{\epsilon}(t)$. For simplicity we only considered molecules oriented such that the laser polarization lay along the x axis for the calculations shown in Fig. 2; however, this ignored couplings due to other laser-molecule projections. In Fig. 3 we start to account for this issue by calculating the x projection (reproduction of Fig. 2) in the top left corner, the y projection in the top right corner, and the z projection in the bottom left corner. A quick comparison of these three panels highlights the fact that the projections have a strong bearing on which states are excited. One can note that for the x projection the same states are populated for the first four photon orders represented. This is not the case for the y projection, which shows that one- and three-photon excitation populates the same states, but two-photon excitation populates entirely different states.

As the aim of these calculations is to aid and inform experimental measurements where the molecules are often randomly oriented, we had to account for the various possible molecule-laser projections. To do this we describe the

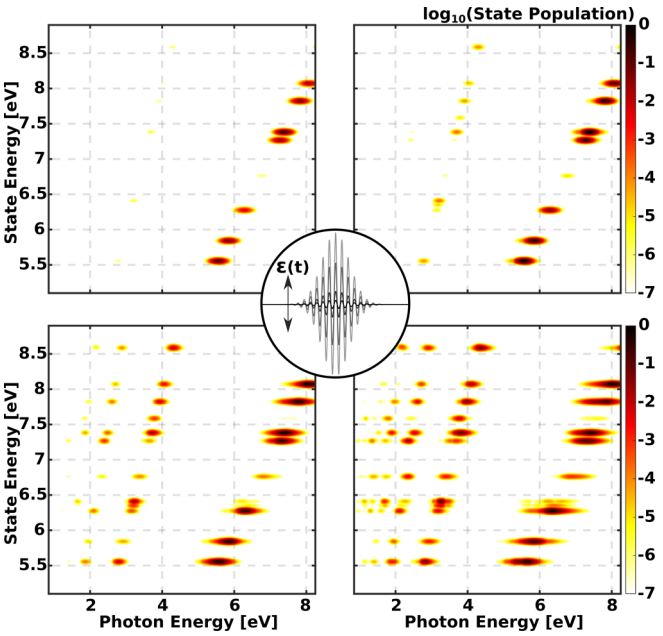

FIG. 4. Rotationally averaged multiphoton spectra for different laser intensities in the FC geometry. Top left: $I = 0.1\,\mathrm{TW/cm^2}$. Top right: $I = 1\,\mathrm{TW/cm^2}$. Bottom left: $I = 10\,\mathrm{TW/cm^2}$. Bottom right: $I = 30\,\mathrm{TW/cm^2}$.

coupling term, $\vec{\mu} \cdot \vec{\epsilon}$ by

$$\vec{\mu} \cdot \vec{\epsilon} = \mu_x \epsilon_0 \sin\theta \cos\phi + \mu_y \epsilon_0 \sin\theta \sin\phi + \mu_z \epsilon_0 \cos\theta, \tag{5}$$

where θ and ϕ are the polar and azimuthal angles, respectively, on the unit sphere depicted in the central cartoon of Fig. 3. We averaged the populations from calculations for a distribution of angles encompassing the sphere to create a rotationally averaged multiphoton spectrum as shown in the bottom right panel of Fig. 3. The states present in the previous three panels for the pure projections are represented in the averaged one, but it is clear that many more states are active here as well.

This approach is necessary because a simple linear combination of the pure projections (x, y, z) lacks multiphoton coupling through the different projections. This is described mathematically by Eqs. (6) and (7), which will be discussed in detail later, but a simple explanation can be found by comparing the one- and two-photon excitations. For the one-photon case, a linear combination of the three pure projections works because one-photon excitation can only couple states through one of the three projections, i.e., excited state C can only be reached if the x, y, or z projection between the ground state A and excited state C is nonzero. However, a two-photon resonance allows coupling between A and C via an intermediate state B even if all three pure projections between A and C are zero. For example, states A and B are one-photon coupled through only the x projection followed by states B and C being one-photon coupled through only the y projection. In this case, just looking at the three pure projections would yield population in state B but never in state C. As the multiphoton order increases, so does the possibility for these types of couplings such that a linear combination of the three pure projections fails for higher-order photon resonances, as is clear from the two- and three-photon orders in the rotationally averaged panel. An example is marked by the dashed white box in Fig. 3 in the region of two-photon absorption. For the three pure projections, there is no two-photon resonance; however, when rotationally averaging we see that there are several two-photon resonances. This effect exists for all multiphoton orders.

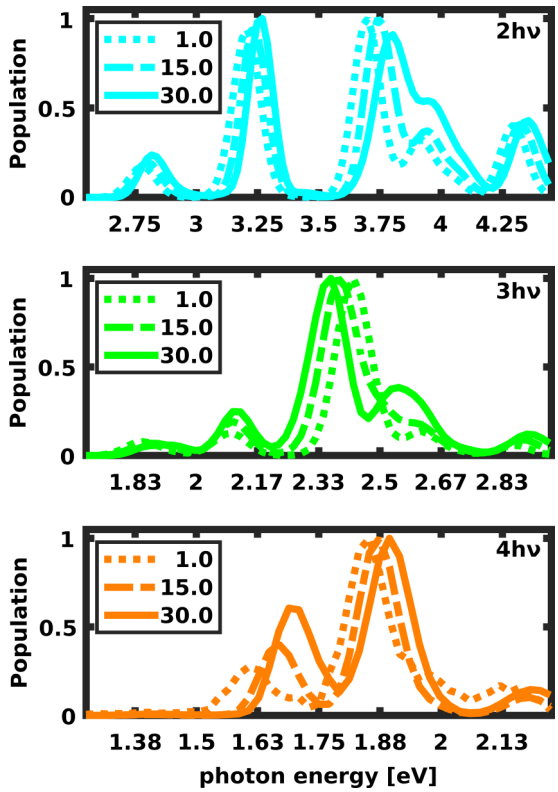

FIG. 5. Multiphoton absorption spectra (lineouts) for different laser intensities. The three panels show the two (top panel), three (middle panel), and four (bottom panel) photon absorption as a function of photon energy for three different laser intensities ($I = 1\,\mathrm{TW/cm^2}$, $I = 15\,\mathrm{TW/cm^2}$, $I = 30\,\mathrm{TW/cm^2}$), illustrating the effect of dynamic Stark shifts.

B. Stark shifting

Next we consider the intensity dependence of these multiphoton spectra. Figure 4 highlights these results. The top left panel shows the calculations for a laser intensity of $0.1\,\mathrm{TW/cm^2}$, with single-photon transitions dominating the spectrum. As the intensity is increased to $1\,\mathrm{TW/cm^2}$ (top right panel), $10\,\mathrm{TW/cm^2}$ (bottom left panel), and $30\,\mathrm{TW/cm^2}$ (bottom right panel) we see higher multiphoton orders appearing. By comparing the first order at 0.1 and $30\,\mathrm{TW/cm^2}$, we can see a spreading of the state populations in photon energy. This spreading comes from the inherent Stark shifting of the states [51].

We can be more quantitative about the Stark shifts by taking multiphoton lineouts for various intensities. Figure 5 shows the two-, three-, and four-photon absorption spectra (lineouts) for three different laser intensities, illustrating how dynamic Stark shifts affect the absorption spectrum. Both

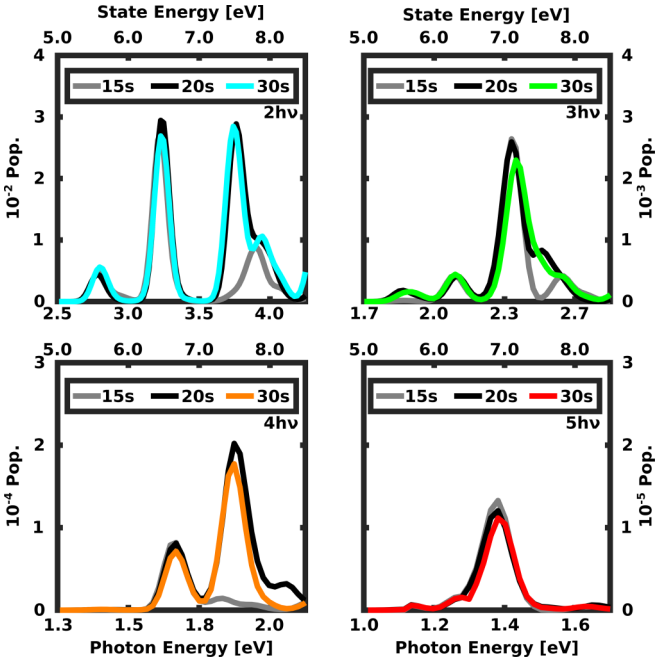

FIG. 6. Comparison of different number of states. The four panels show the multiphoton lineouts for photon orders: two (top left), three (top right), four (bottom left), and five (bottom right). Bottom x axis shows the photon energy and the top x axis shows the state energy. The colored lines correspond to the colors used in Fig. 2 and indicate the $11o30s$ model used throughout the paper.

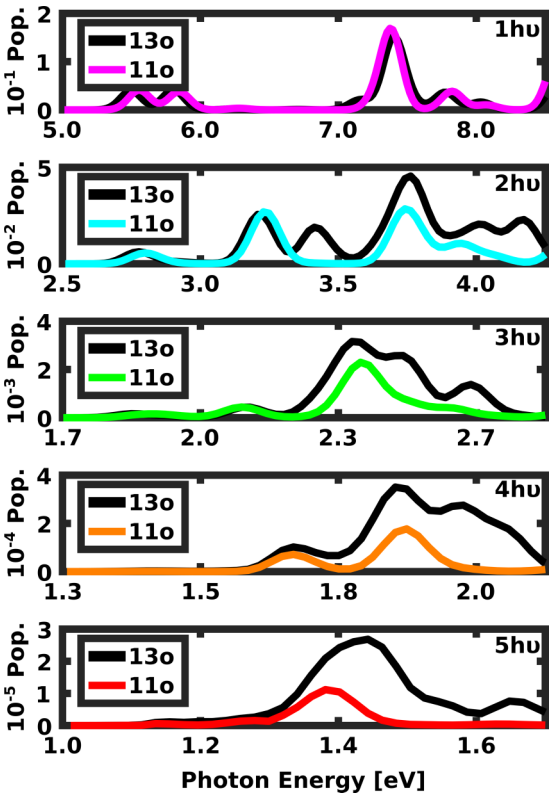

FIG. 7. Comparison of different levels of theory. The five panels show the multiphoton lineouts for photon orders one to five from top to bottom. Bottom x axis shows the photon energy and the top axis shows the state energy. The colored lines correspond to the colors used in Fig. 2 and indicate the $11o30s$ model used throughout the paper.

positive and negative Stark shifts can be observed, with most peaks displaying positive Stark shifts, as one expects in the ponderomotive limit. However, we also observe a negative Stark shift for the highest peak in the three-photon absorption spectrum. Also, we note that the Stark shifts can lead to variations in relative peak heights, as different intermediate states shift closer into resonance, enhancing the absorption of N photons.

C. Model comparison

Another feature of the multiphoton calculations is that they offer a test of the robustness of the electronic structure calculations beyond what one can gather from the linear absorption spectrum. When running electronic structure calculations with multiconfigurational wave functions, one has to choose the number of states, and the size of the active space. Enlarging an active space (without exchanging orbitals) usually provides more precision, but comes at the cost of computation time, so one often has to sacrifice precision for realistic computation times. Increasing the number of considered states increases the accuracy of the multiphoton calculation, i.e., the outcome of the TDSE computation, while a slight decrease in the quality of the state energies in the electronic structure calculations due to a state average over more states is usually negligible in comparison.

We first consider the number of electronic states that are included. In Fig. 6 we show the second- through fifth-order multiphoton lineouts for models including 15, 20, and 30 electronic states. All three models show the the same peaks in the multiphoton absorption spectra for state energies below 7 eV. Above this value we see that the 15 state model differs significantly from the 20 and 30 state models. For instance, the 15 state model completely misses the 1.9 eV resonance at fourth order. The 20 state and 30 state models are quite comparable for all four orders suggesting that the 30 state model captures the "essential states" and we do not need an infinite number of states to model the dynamics for the laser pulses considered here.

Another key aspect of these types of electronic structure calculations is the number of orbitals over which the electrons are distributed. In Fig. 7 we compare the multiphoton absorption spectra for two models containing 11 and 13 orbitals for the same number of electronic states (30). The top panel shows the single-photon absorption spectrum, where there is good agreement between the two models. But even at the next photon order we start to see significant discrepancies between the two models. One would expect that increasing the number of orbitals should increase the precision, but this would require a subsequent increase in the number of electronic states, which becomes computationally restrictive. Earlier efforts by Roos *et al.* [40] were able to get around this issue by keeping the desired orbitals separate and ran two independent large active space calculations which they combined later on. This is an excellent approach for them as they wished to calculate the single-photon absorption spectrum,

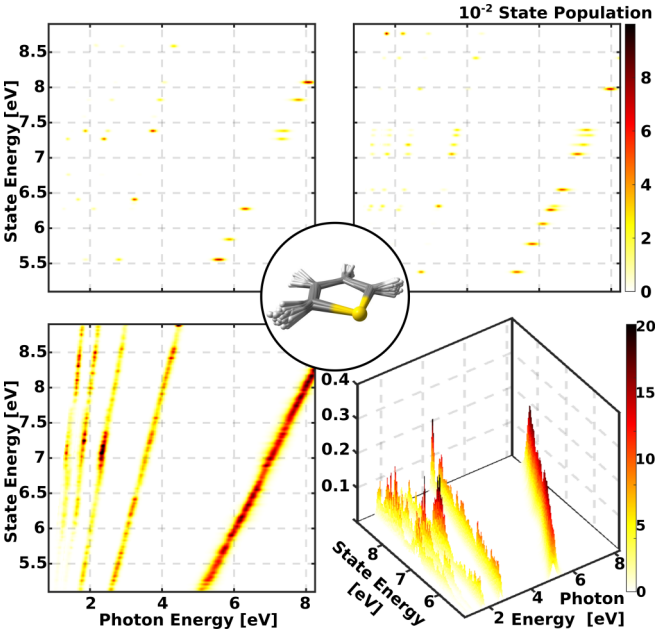

FIG. 8. Rotationally averaged multiphoton spectra for different molecular geometries. Top left: Franck-Condon geometry. Top right: A structure randomly chosen from the Wigner distribution of geometries around the Franck-Condon geometry. Bottom left: Average over 200 Wigner-distributed geometries. Bottom right: Same as bottom left, different view. Note that the color axis uses a linear scale to emphasize the differences in Wigner-averaged spectrum, which means that to allow the multiphoton orders to be visible we scaled the population in the first order by 10 and each order subsequent order, n, by 10^{n-1}.

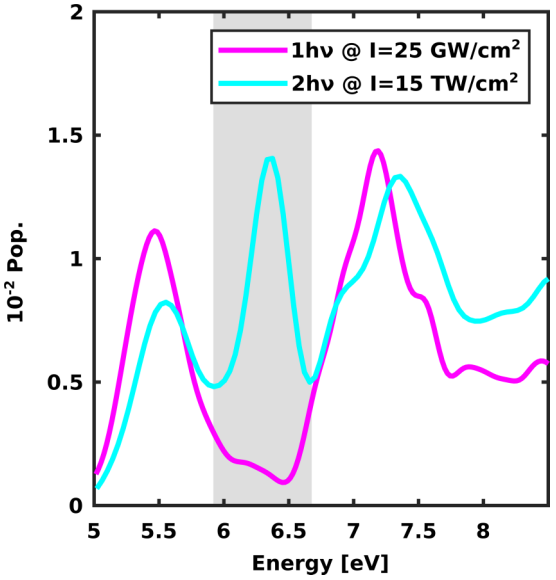

FIG. 9. One- versus two-photon absorption. This figure illustrates the ability to populate one-photon dark states via multiphoton absorption. Note the two-photon absorption peak at about 6.3 eV, which is absent in the single-photon absorption spectrum.

but it poses a similar problem for us as the one we faced with rotationally averaging. Since the two computations are split they did not provide the transition dipole moments between all of the calculated states, which means that we would be missing out on several multiphoton transitions. In addition, splitting the quantum chemical calculations, as was done in Ref. [40], is based on splitting the active spaces themselves, which relies on molecular symmetry and a careful selection of orbitals in the different active spaces. This is prohibited when the calculations are to be performed for multiple, possibly for a large number of, nonsymmetric geometries beyond the FC. This, however, is necessary for computing multiphoton spectra, as discussed below.

D. Wigner distribution

The electronic structure calculations provide us with the state energies and transition dipole moments assuming a fixed molecular geometry. Up to this point, we only dealt with the FC geometry. In the top left panel of Fig. 8 we show the rotationally averaged multiphoton spectrum for the FC geometry as discussed previously in Fig. 3. We repeat the multiphoton calculation for a different randomly distorted geometry (DG) of the molecule under the same conditions as the FC geometry presented in the top right panel of Fig. 8. There are clear differences between these two multiphoton spectra, not simply in what states are excited, but also in the extent to which each state is excited. To investigate why the DG spectra shows excitation to many more states, we ran the multiphoton calculation again swapping the transition dipole moments for the two geometries. By making this swap we were able to determine that the increase in excitations are due to the transition dipole moments. The nonidealized (not FC) geometry breaks the molecular symmetry leading to more nonzero transition dipole moment elements thus excitation to more states.

With this in mind, it becomes necessary to sample molecular geometries to accurately model the system [22], in other words calculate a Wigner distribution [52]. We did exactly this for a number of different geometries and summed the populations across all geometries to produce a Wigner-averaged multiphoton spectrum. It is necessary to sample a large number of molecular geometries for the Wigner-averaged multiphoton spectrum to converge. We find that averaging up to 200 geometries leads to reasonable qualitative convergence of the main features of the multiphoton spectrum. While in the top two panels of Fig. 8 we show the spectrum for the FC and DG geometries discussed, in the bottom panels we show the multiphoton spectrum averaged over all 200 geometries sampled from the Wigner distribution. In these bottom panels we show the results on a linear scale. To allow the multiphoton orders to be visible, we scaled the population in the first order by 10 and each subsequent order, n, by 10^{n-1}. The bottom left panel shows a top-down view of the Wigner-averaged spectrum, while the right panel shows a three-dimensional (3D) version of the same spectrum.

Due to the high intensity required for the higher photon orders to appear, the one-photon spectrum is saturated in this figure. However, we are more interested in the higher-photon orders which show clear peaks. This is more clearly seen in the 3D view, where the three-photon order has a prominent peak at around 7 eV, for example. While averaging over many geometries in the Wigner distribution broadens the features

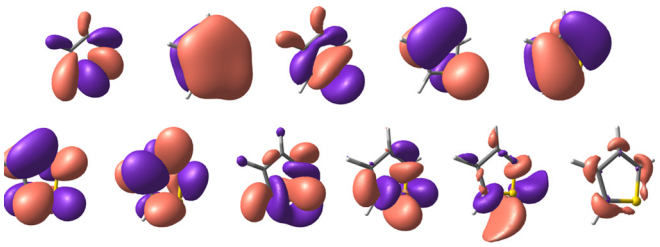

FIG. 10. Shapes of active electron orbitals at the Franck-Condon geometry. Upper row: Orbitals doubly occupied in ground state. Lower row: Empty orbitals in ground state. The orbitals were all displayed with the same contour value.

in the multiphoton absorption spectrum, there are still peaks, and they display Stark comparable to those we discussed for the FC geometry in Sec. III B, as shown in Fig. 11.

A simple check of our calculations is to compare the calculations for low intensities with the single-photon absorption spectrum generated by the oscillator strengths, and experimental data. This comparison is shown in Fig. 12, discussed in the Appendix, and demonstrates excellent agreement. With this fully rotationally and Wigner-averaged spectrum we can now look towards new experimental measurements.

E. Applications

The calculations described above can have many applications, but one avenue in particular that we are exploring is studying one-photon dark states. In Fig. 9 we show one- and two-photon absorption spectra using full rotational and Wigner averaging. Both spectra reproduce the states at 5.5 eV and 7.2 eV where the two-photon absorption spectra is undergoing a Stark shift due to the 600 times increase in laser intensity. The most interesting feature is that the two-photon absorption spectra shows an additional peak at 6.3 eV. This highlights the ability to populate one-photon dark states via multiphoton absorption.

The ability to populate one-photon dark states via multiphoton absorption can be understood by comparing the one- and two-photon coupling. For single-photon transitions, the coupling is driven by the transition dipole matrix element

$$\chi_{i,j}(t) \propto \langle \psi_i | \vec{\mu} \cdot \vec{\varepsilon}(t) | \psi_j \rangle. \tag{6}$$

For two-photon transitions, the coupling is driven by a sum of products of transition dipole matrix elements

$$\chi_{i,j}(t) \propto \sum_k \langle \psi_i | \vec{\mu} \cdot \vec{\varepsilon}(t) | \psi_k \rangle \langle \psi_k | \vec{\mu} \cdot \vec{\varepsilon}(t) | \psi_j \rangle. \tag{7}$$

Note that this sum of products contains cross terms in the different x, y, and z projections of the laser field on the molecular transition dipole moment, as noted in the rotational averaging discussion above (see Sec. III A). There can be situations where the single-photon coupling vanishes due to symmetry or wave-function overlap, but the two- or multiphoton coupling does not because of the involvement of intermediate off-resonant states, which can serve as a bridge between nonoverlapping states. In the specific case we consider here, the single-photon coupling is low due to poor wave-function overlap.

IV. CONCLUSION

In conclusion, we present calculations of multiphoton molecular absorption using a combination of *ab initio* electronic structure calculations and essential states calculations of the light-matter interaction for a strong few-cycle laser

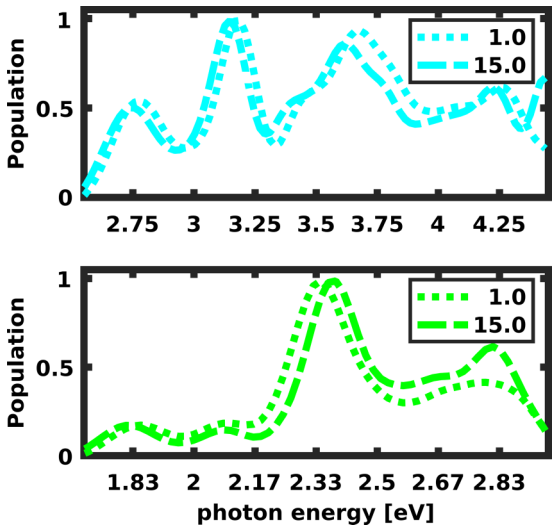

FIG. 11. Multiphoton absorption spectra (lineouts) for different laser intensities for Wigner-averaged data. The two panels show the two (top panel) and three (bottom panel) photon absorption as a function of photon energy for two different laser intensities ($I = 1\,\mathrm{TW/cm^2}$, $I = 15\,\mathrm{TW/cm^2}$), illustrating the effect of dynamic Stark shifts.

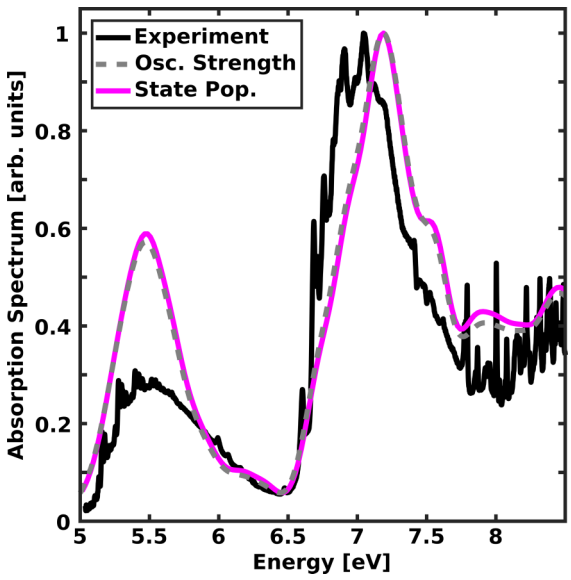

FIG. 12. Linear absorption spectrum for thiophene experimentally measured (solid black) reproduced from Holland *et al.* [53], calculated from the oscillator strengths from a Wigner-sampled electronic structure calculation (dashed gray), and calculated from the solution to the TDSE with Wigner-sampled initial conditions (solid magenta). For comparison of the populations and the oscillator strengths, the populations are scaled by the photon energy.

pulse. The calculations illustrate the ability to excite multiple states of the molecule in less than a vibrational period through multiphoton absorption, which can populate single-photon dark states, which are difficult to study otherwise. As a general approach, which only requires input from straightforward electronic structure calculations, we hope that this may help to guide and interpret many future time-resolved measurements that require multiphoton excitation or probing.

ACKNOWLEDGMENTS

We gratefully acknowledge helpful discussions with Thomas Wolf. This work was supported by the National Science Foundation under Award No. 1806294. T. Rozgonyi acknowledges support from the Government of Hungary and the European Regional Development Fund under Grant No. VEKOP-2.3.2-16-2017-00015 and also from the Hungarian National Research, Development and Innovation Fund under Grant No. SNN 135636.

APPENDIX

Here we present additional details for the electronic structure calculations in regards to the Franck-Condon (FC) geometry. In Table I we outline the coordinates for each atom of thiophene in the FC geometry, where the molecule is planar and lays in the *xy* plane. In Fig. 10 we show the shapes of active electron orbitals at the FC geometry. The upper row shows the orbitals, which are doubly occupied in ground state, while the lower row shows empty orbitals in the ground state.

Here we show the Stark shifting of the peaks in the multiphoton absorption spectra for Wigner-averaged data. We can see that the Stark shifting is comparable to the Stark shifts presented in Fig. 5, which was solely for the FC geometry.

A standard test of electronic structure calculations is to compare the oscillator strengths as a function of energy or wavelength with the experimentally measured absorption spectrum. The oscillator strengths are calculated from the energies and transition dipole moments generated from the electronic structure calculations. These are the same parameters that are used as input into our quantum dynamics calculations, so one would expect that the linear absorption spectrum from both calculations should be comparable. To make this comparison, we solved the TDSE for the full rotationally averaged Wigner distribution at an intensity low enough to remain in the perturbative limit. Figure 12 shows the results of this calculation. Here we reproduce the experimentally measured linear absorption spectrum for thiophene from Holland *et al.* [53] in black. The absorption spectrum calculated from the oscillator strengths from a Wigner-sampled electronic structure calculation is shown in dashed gray and calculated from the solution to the TDSE with Wigner-sampled initial conditions is shown in solid magenta. For a direct comparison to the absorption spectrum and the oscillator strengths, the populations from the quantum dynamics calculations had to be scaled by the photon energy. The absorption spectrum from the quantum dynamics calculations is nearly identical to that of the electronic structure calculations emphasizing that the quantum dynamics calculations behave as expected. In addition, both spectra also compare quite well to the experimental absorption spectrum, reproducing the main two peaks at 5.5 eV and 7 eV.

TABLE I. Franck-Condon geometry of thiophene. The molecule is planar and lays in the *xy* plane. Coordinates are given in Å.

Atom	*x* coord.	*y* coord.
S	−1.193	0.000
C	0.009	−1.238
C	0.009	1.238
C	1.267	−0.712
C	1.267	0.712
H	−0.282	−2.274
H	−0.282	2.274
H	2.163	−1.314
H	2.163	1.314

[1] P. R. Bunker and P. Jensen, *Molecular Symmetry and Spectroscopy* (NRC Research Press, Ottawa, 2006),Vol. 46853.
[2] W. L. Peticolas, Annu. Rev. Phys. Chem. **18**, 233 (1967).
[3] J. Bhawalkar, G. He, and P. Prasad, Rep. Prog. Phys. **59**, 1041 (1996).
[4] M. Rumi and J. W. Perry, Adv. Opt. Photonics **2**, 451 (2010).
[5] T. Weinacht and B. Pearson, *Time-Resolved Spectroscopy: An Experimental Perspective* (CRC, Boca Raton, FL, 2019), pp. 43–52.
[6] A. Stolow, A. E. Bragg, and D. M. Neumark, Chem. Rev. **104**, 1719 (2004).
[7] M. Ashfold and J. Howe, Annu. Rev. Phys. Chem. **45**, 57 (1994).
[8] A. M. Larson, Nat. Photonics. **5**, 1 (2011).
[9] B. W. Shore, *The Theory of Coherent Atomic Excitation: Multilevel Atoms and Incoherence*, Vol. 2 (Wiley-Interscience, New York, 1990), p. 1736.
[10] E. Brion, L. H. Pedersen, and K. Mølmer, J. Phys. A: Math. Theor. **40**, 1033 (2007).
[11] M. Krug, T. Bayer, M. Wollenhaupt, C. Sarpe-Tudoran, T. Baumert, S. S. Ivanov, and N. V. Vitanov, New J. Phys. **11**, 105051 (2009).
[12] B. Kaufman, T. Rozgonyi, P. Marquetand, and T. Weinacht, Phys. Rev. A **102**, 063117 (2020).
[13] W. D. M. Lunden, P. Sándor, T. C. Weinacht, and T. Rozgonyi, Phys. Rev. A **89**, 053403 (2014).
[14] M. Göppert-Mayer, Ann. Phys. (Leipzig) **401**, 273 (1931).
[15] V. Paulisch, H. Rui, H. K. Ng, and B.-G. Englert, Eur. Phys. J. Plus **129**, 12 (2014).
[16] TURBOMOLE V6.2 2010, a development of University of Karlsruhe and Forschungszentrum Karlsruhe GmbH, 1989–2007, TURBOMOLE GmbH, since 2007; available from http://www.turbomole.com, 2012.
[17] F. Neese, WIREs Comput. Mol. Sci. **2**, 73 (2012).

[18] H.-J. Werner, P. J. Knowles, G. Knizia, F. R. Manby, and M. Schütz, WIREs Comput. Mol. Sci. **2**, 242 (2012).
[19] I. F. Galván, M. Vacher, A. Alavi, C. Angeli, F. Aquilante, J. Autschbach, J. J. Bao, S. I. Bokarev, N. A. Bogdanov, R. K. Carlson, L. F. Chibotaru, J. Creutzberg, N. Dattani, M. G. Delcey, S. S. Dong, A. Dreuw, L. Freitag, L. M. Frutos, L. Gagliardi, F. Gendron, A. Giussani *et al.*, J. Chem. Theory Comput. **15**, 5925 (2019).
[20] S. Mai, P. Marquetand, and L. González, WIREs Comput. Mol. Sci. **8**, e1370 (2018).
[21] M. Barbatti, M. Ruckenbauer, F. Plasser, J. Pittner, G. Granucci, M. Persico, and H. Lischka, WIREs Comput. Mol. Sci. **4**, 26 (2014).
[22] J. Westermayr and P. Marquetand, J. Chem. Phys. **153**, 154112 (2020).
[23] V. Tagliamonti, B. Kaufman, A. Zhao, T. Rozgonyi, P. Marquetand, and T. Weinacht, Phys. Rev. A **96**, 021401(R) (2017).
[24] M. Koch, T. J. A. Wolf, and M. Gühr, Phys. Rev. A **91**, 031403(R) (2015).
[25] B. Kaufman, T. Rozgonyi, P. Marquetand, and T. Weinacht, Phys. Rev. Lett. **125**, 053202(R) (2020).
[26] J. A. Sell and A. Kuppermann, Chem. Phys. Lett. **61**, 355 (1979).
[27] G. Turkoglu, M. E. Cinar, and T. Ozturk, Top. Curr. Chem (Z) **375**, 84 (2017).
[28] B. L. Rupert, W. J. Mitchell, A. J. Ferguson, M. E. Köse, W. L. Rance, G. Rumbles, D. S. Ginley, E. S. Shaheen, and N. Kopidakis, J. Mater. Chem. **19**, 5311 (2009).
[29] P. M. Beaujuge and J. M. J. Fréchet, J. Am. Chem. Soc. **133**, 20009 (2011).
[30] I. F. Perepichka, D. F. Perepichka, H. Meng, and F. Wudl, Adv. Mater. **17**, 2281 (2005).
[31] J. Shi, Y. Li, M. Jia, L. Xu, and H. Wang, Org. Electron. **14**, 934 (2013).
[32] H. Köppel, E. Gromov, and A. Trofimov, Chem. Phys. **304**, 35 (2004).
[33] S. Salzmann, M. Kleinschmidt, J. Tatchen, R. Weinkauf, and C. M. Marian, Phys. Chem. Chem. Phys. **10**, 380 (2008).
[34] A. Prlj, B. F. E. Curchod, and C. Corminboeuf, Phys. Chem. Chem. Phys. **17**, 14719 (2015).
[35] T. Schnappinger, P. Kölle, M. Marazzi, A. Monari, L. González, and R. de Vivie-Riedle, Phys. Chem. Chem. Phys. **19**, 25662 (2017).
[36] M. Dash, S. Moroni, C. Filippi, and A. Scemama, J. Chem. Theory Comput. **17**, 3426 (2021).
[37] P. Sándor, V. Tagliamonti, A. Zhao, T. Rozgonyi, M. Ruckenbauer, P. Marquetand, and T. Weinacht, Phys. Rev. Lett. **116**, 063002 (2016).
[38] C. Cheng, Z. L. Streeter, A. J. Howard, M. Spanner, R. R. Lucchese, C. W. McCurdy, T. Weinacht, P. H. Bucksbaum, and R. Forbes, Phys. Rev. A **104**, 023108 (2021).
[39] J. Finley, P. Malmqvist, B. O. Roos, and L. Serrano-Andrés, Chem. Phys. Lett. **288**, 299 (1998).
[40] L. Serrano-Andrés, M. Manuela, M. Fülscher, and B. O. Roos, Chem. Phys. Lett. **211**, 125 (1993).
[41] P. Kölle, T. Schnappinger, and R. de Vivie-Riedle, Phys. Chem. Chem. Phys. **18**, 7903 (2016).
[42] P.-O. Widmark, P.-A. Malmqvist, and B. O. Roos, Theor. Chim. Acta **77**, 291 (1990).
[43] B. O. Roos, R. Lindh, P.-A. Malmqvist, V. Veryazov, and P.-O. Widmark, J. Phys. Chem. A **109**, 6575 (2005).
[44] M. Reiher, WIREs Comput. Mol. Sci. **2**, 139 (2012).
[45] P. A. Malmqvist, B. O. Roos, and B. Schimmelpfennig, Chem. Phys. Lett. **357**, 230 (2002).
[46] A. D. Becke, J. Chem. Phys. **98**, 5648 (1993).
[47] C. Lee, W. Yang, and R. G. Parr, Phys. Rev. B **37**, 785 (1988).
[48] K. A. Peterson, D. Figgen, E. Goll, H. Stoll, and M. Dolg, J. Chem. Phys. **119**, 11113 (2003).
[49] M. J. Frisch, G. W. Trucks, H. B. Schlegel, G. E. Scuseria, M. A. Robb, J. R. Cheeseman, G. Scalmani, V. Barone, B. Mennucci, G. A. Petersson *et al.*, *Gaussian 09* (Gaussian Inc., Wallingford, CT, 2009).
[50] S. Mai, M. Richter, M. Heindl, M. F. S. J. Menger, A. Atkins, M. Ruckenbauer, F. Plasser, L. M. Ibele, S. Kropf, O. Markus, P. Marquetand, and L. González, *SHARC 2.1: Surface Hopping Including Arbitrary Couplings - Program Package for Non-Adiabatic Dynamics*, 2019, http://www.sharc-md.org.
[51] D. J. Tannor, *Introduction to Quantum Mechanics : A Time-Dependent Perspective* (University Science Books, Sausolito, CA, 2007).
[52] E. Wigner, Phys. Rev. **40**, 749 (1932).
[53] D. M. P. Holland, A. B. Trofimov, E. A. Seddon, E. V. Gromov, T. Korona, N. de Oliveira, L. E. Archer, D. Joyeux, and L. Nahon, Phys. Chem. Chem. Phys. **16**, 21629 (2014).